AAAS
Research
Volume 2019, Article ID 5173580, 8 pages
https://doi.org/10.34133/2019/5173580

Research
A SCIENCE PARTNER JOURNAL

Research Article

Three-Dimensional Topological States of Phonons with Tunable Pseudospin Physics

Yizhou Liu[1,2,3], Yong Xu[1,2,3], and Wenhui Duan[1,2,4]

[1]*State Key Laboratory of Low Dimensional Quantum Physics, Department of Physics, Tsinghua University, Beijing 100084, China*
[2]*Collaborative Innovation Center of Quantum Matter, Beijing 100084, China*
[3]*RIKEN Center for Emergent Matter Science (CEMS), Wako, Saitama 351-0198, Japan*
[4]*Institute for Advanced Study, Tsinghua University, Beijing 100084, China*

Correspondence should be addressed to Yong Xu; yongxu@mail.tsinghua.edu.cn

Received 8 June 2019; Accepted 5 July 2019; Published 31 July 2019

Copyright © 2019 Yizhou Liu et al. Exclusive Licensee Science and Technology Review Publishing House. Distributed under a Creative Commons Attribution License (CC BY 4.0).

Efficient control of phonons is crucial to energy-information technology, but limited by the lacking of tunable degrees of freedom like charge or spin. Here we suggest to utilize crystalline symmetry-protected pseudospins as new quantum degrees of freedom to manipulate phonons. Remarkably, we reveal a duality between phonon pseudospins and electron spins by presenting Kramers-like degeneracy and pseudospin counterparts of spin-orbit coupling, which lays the foundation for "pseudospin phononics". Furthermore, we report two types of three-dimensional phononic topological insulators, which give topologically protected, gapless surface states with linear and quadratic band degeneracies, respectively. These topological surface states display unconventional phonon transport behaviors attributed to the unique pseudospin-momentum locking, which are useful for phononic circuits, transistors, antennas, etc. The emerging pseudospin physics offers new opportunities to develop future phononics.

Recently intensive research effort has been devoted to finding novel topological states of phonons, including the quantum anomalous Hall-like [1–15] and quantum spin Hall-like states [16–21]. These new quantum states of phonons are characterized by topologically protected, gapless boundary modes within the bulk gap, which are useful for various applications like high-efficiency phononic circuits/diodes and offer new paradigms for future phononics [12–14]. However, experimental realization of two-dimensional (2D) topological states is quite challenging for phonon systems. Specifically, the quantum anomalous Hall-like states require breaking time reversal symmetry of phonons, which remains experimentally illusive. The quantum spin Hall-like states rely on the pseudospin degeneracy protected by crystalline symmetries that typically get broken at the one-dimensional (1D) edges [21]. In contrast, crystalline symmetries of three-dimensional (3D) systems can preserve simultaneously in the bulk and on the surface, enabling the topological protection. Importantly, most solid materials are crystalized in 3D lattices. Nevertheless, despite a few preliminary works on phononic topological semimetals [22–25], 3D phononic topological insulators (TIs) have rarely been reported before, as far as we know. This is possibly because the spin (Kramers) degeneracy and spin-orbit coupling (SOC), which are essential to TIs, are natively missing for phonons. On the other hand, phonons are elementary excitations of lattice vibrations with zero charge and spin. The lacking of tunable degrees of freedom considerably limits their device applications. In this context, it is of critical importance to develop new quantum degrees of freedom for phonons. In light of the great success of spintronics, future research of phononics would be greatly enriched if one could establish any correlations between phonon pseudospins and electron spins [26].

In this Article, we provided a guiding principle to design 3D phononic TIs as well as topological semimetals by utilizing crystalline symmetry-protected pseudospins characterized by Kramers-like degeneracy, quantized pseudoangular momenta, and nonzero Berry curvature. Remarkably, we revealed pseudospin counterparts of the intrinsic and Rashba-Dresselhaus SOC, namely, the pseudo-SOC of phonons, which builds a duality between phonon pseudospins and electron spins. The duality feature enables exploring the physics and applications of phonon

pseudospins by borrowing ideas from spintronics, thus opening new opportunities for "pseudospin phononics".

1. Design Principle of Phononic TIs

An essential requirement of TIs is band degeneracies at no less than two high symmetry momenta (HSM) in the boundary Brillouin zone (BZ) [27–29]. The requirement is satisfied for electrons with spin degeneracies protected by time reversal symmetry. However, phonons do not have real spins, invoking different strategies for building phononic TIs. Naturally one could apply crystalline symmetries that are prevalent in solid materials to realize Kramers-like degeneracies. Such symmetries should also be preserved when projected onto the surface. However, for 2D spinless cases, no such kind of crystalline symmetry has higher than 1D irreducible representations at more than one HSM in the 1D edge BZ, implying that 2D phononic TIs protected by crystalline symmetries are forbidden [21]. The constraint is released for a variety of 3D lattices, where multiple band degenerate HSM can exist in the 2D surface BZ [28–31]. Thus the construction of 3D phononic TIs is feasible in principle.

The Hamiltonian of phonons resembles a tight-binding Hamiltonian of spinless electrons with fixed $p_{x,y,z}$ orbitals [13]. The symmetry representation of phonons is $\Gamma_{\text{phonon}} = \Gamma^{\text{equiv.}} \otimes \Gamma_{\text{vector}}$, where $\Gamma^{\text{equiv.}}$ is the equivalence representation of atomic sites and Γ_{vector} is the representation of a 3D polar vector [32]. Here we will not thoroughly discuss all possible 3D crystalline symmetries, but focus on C_{nv} ($n = 3, 4, 6$) symmetries that show interesting topological physics for electrons [30, 31]. Take C_{6v} lattices as an example. $\Gamma^{\text{equiv.}}$ is a N dimensional representation, where N is the number of atomic sites in a unit cell. When all the atomic sites are inequivalent, $\Gamma^{\text{equiv.}}$ is decomposed into N 1D irreducible representations A_1. $N \geq 2$ is necessary to build a phononic TI that requires at least four bands. For simplicity, we choose $N = 2$ as displayed in Figure 1(a), which gives $\Gamma^{\text{equiv.}} = 2A_1$. In the momentum space, the high-symmetry lines Γ-A and K-H in the bulk BZ are projected onto the HSM $\overline{\Gamma}$ and $\overline{K}$ in the surface BZ [Figure 1(a)], which have C_{6v} and C_{3v} symmetries, respectively. Under $C_{6(3)v}$ symmetry, $\Gamma_{\text{vector}} = A_1 \oplus E$, where A_1 and E are 1D and 2D irreducible representations for basis functions of p_z and $p_x \pm ip_y$, respectively. Therefore, $\Gamma_{\text{phonon}} = 2A_1 \oplus 2E$, implying that $p_x \pm ip_y$ (p_z) are doubly degenerate (nondegenerate) along the high-symmetry lines. Note that frequencies of in-plane vibrations ($p_x \pm ip_y$) are typically higher than those of out-of-plane ones (p_z), leading to weak hybridization between the doublet and singlet states. We thus focus on in-plane vibrations [33], for which a $\mathbb{Z}_2$ classification of band topology is permitted [30].

2. Pseudospin- and Topology-Related Physics

Considering that the double degeneracy of $p_x \pm ip_y$ resembles the Kramers degeneracy of spins, we introduce a pseudospin index to label the Kramers-like states. There exist two types of phonon modes, including in-phase (I) and out-of-phase (O) vibrations between the two atomic sites A and B. Their pseudospin states [Figure 1(b)] are defined in coordinates of $(x_A, y_A, x_B, y_B)^T$ as

$$\begin{aligned} \left|\mathrm{I}_{\uparrow}\right\rangle &= \left(\varepsilon_+ \sin\theta_{\mathbf{k}}, \varepsilon_+ \cos\theta_{\mathbf{k}}\right)^T, \\ \left|\mathrm{O}_{\uparrow}\right\rangle &= \left(\varepsilon_- \cos\theta_{\mathbf{k}}, -\varepsilon_- \sin\theta_{\mathbf{k}}\right)^T, \\ \left|\mathrm{I}_{\downarrow}\right\rangle &= i\left(\varepsilon_- \sin\theta_{\mathbf{k}}, \varepsilon_- \cos\theta_{\mathbf{k}}\right)^T, \\ \left|\mathrm{O}_{\downarrow}\right\rangle &= i\left(-\varepsilon_+ \cos\theta_{\mathbf{k}}, \varepsilon_+ \sin\theta_{\mathbf{k}}\right)^T, \end{aligned} \tag{1}$$

where $\varepsilon_\pm = (1, \pm i)/\sqrt{2}$ and the vibrational magnitude of each atomic site is determined by $\theta_{\mathbf{k}} \in [0, \pi/2]$ that is $\mathbf{k}$-dependent. They are orthonormal and form a complete basis of in-plane vibrations.

The pseudospin states are featured by well-defined, quantized pseudoangular momenta about z-axis for $\mathbf{k}$ along the high-symmetry lines due to the $C_{6(3)}$ rotational symmetry. The pseudoangular momentum operator is expressed as $J_{\text{ph}} = \sigma_z s_z$ [33], where σ_z and s_z are Pauli matrices with $\sigma_z = \pm 1$ and $s_z = \pm 1$ refer to pseudospin up (down) and I (O) vibrational modes, respectively. The phonon pseudoangular momentum j_{ph} is composed of two parts, including a local part determined by the on-site orbital and a nonlocal part contributed by the inter-site Bloch phase change [34]. Herein the nonlocal part is zero and j_{ph} is fully determined by the local part, giving $j_{\text{ph}} = 1$ for $|\mathrm{I}_\uparrow\rangle$ and $|\mathrm{O}_\downarrow\rangle$ and $j_{\text{ph}} = -1$ for $|\mathrm{I}_\downarrow\rangle$ and $|\mathrm{O}_\uparrow\rangle$, as depicted in Figure 1(b).

The symmetry-adapted $k \cdot p$ method was applied to derive effective Hamiltonians of phonons near HSM by using the basis set $\{|\mathrm{I}_\uparrow\rangle, |\mathrm{O}_\uparrow\rangle, |\mathrm{I}_\downarrow\rangle, |\mathrm{O}_\downarrow\rangle\}$ [33]. Specifically, the Bloch Hamiltonian matrix $H(\mathbf{k})$ was first expanded by the lowest orders of $\mathbf{k}$ (referenced to HSM). Then, by writing down the corresponding matrices of symmetry operators and requiring $H(\mathbf{k})$ commute with them, some matrix elements of $H(\mathbf{k})$ are enforced to be zero. The remaining nonzero part gives the effective Hamiltonian. The HSM are classified into type-I (K/K' and H/H') and type-II (Γ and A), which have C_{3v} and C_{6v} symmetries, respectively, and will be discussed separately. Importantly, the conservation of pseudoangular momentum requires that basis states of the same j_{ph} (e.g., $|\mathrm{I}_\uparrow\rangle$ and $|\mathrm{O}_\downarrow\rangle$) are coupled only by terms like k_z, $k_x^2 + k_y^2$, and k_z^2, while basis states of different j_{ph} (e.g., $|\mathrm{I}_\uparrow\rangle$ and $|\mathrm{O}_\uparrow\rangle$) are coupled only by terms like $k_\pm$ and $k_\pm^2$. The effective Hamiltonian near the type-I HSM is written as $H = H_0 + H_I + H_{RD}$, where $H_0 = \mathrm{diag}(M_{\mathbf{k}}, -M_{\mathbf{k}}, M_{\mathbf{k}}, -M_{\mathbf{k}})$,

$$\begin{aligned} H_I &= \begin{pmatrix} 0 & \Delta_1 k_+ & 0 & \Delta_2 k_z \\ \Delta_1 k_- & 0 & \Delta_2 k_z & 0 \\ 0 & \Delta_2 k_z & 0 & -\Delta_1 k_- \\ \Delta_2 k_z & 0 & -\Delta_1 k_+ & 0 \end{pmatrix}, \\ H_{RD} &= \begin{pmatrix} 0 & 0 & -iC_1 k_+ & 0 \\ 0 & 0 & 0 & iC_2 k_- \\ iC_1 k_- & 0 & 0 & 0 \\ 0 & -iC_2 k_+ & 0 & 0 \end{pmatrix}, \end{aligned} \tag{2}$$

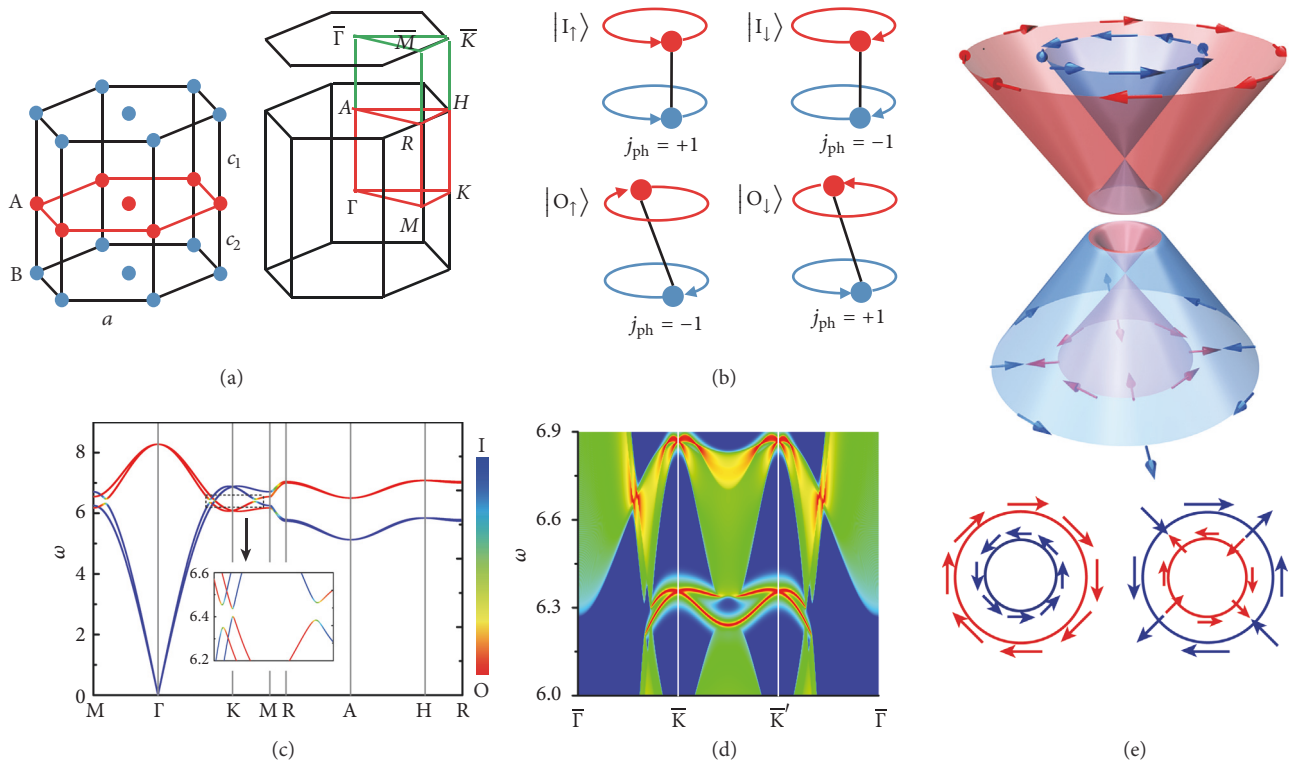


FIGURE 1: (a) Atomic structure (left) and Brillouin zone (right) of a 3D triangular lattice with two sublattices A and B. Bond lengths are denoted by lattice parameters a, c_1, and c_2. (b) Schematic pseudospin states of in-phase "I" (out-of-phase "O") vibrational modes, whose pseudoangular momentum j_{ph} is labelled. (c) Dispersion curves of a type-I phononic TI. Blue (red) color is used to denote the contribution of I (O) vibrational modes. (d) Local density of states (LDOS) of the (001) surface, where higher (lower) LDOS are colored red (blue). (e) Schematic phonon dispersion and pseudospin textures in the $k_z = 0$ plane near K. The bottom panel displays pseudospin textures of O (left) and I (right) vibrational modes from the top view.

$M_{\mathbf{k}} = M - B_1(k_x^2 + k_y^2) - B_2 k_z^2$, $k_\pm = k_x \pm ik_y$. The curvature parameters B_1 and B_2 typically have the same sign.

Remarkably, this effective Hamiltonian resembles the 3D Bernevig-Hughes-Zhang (BHZ) model with broken inversion symmetry for electrons. $H_0 + H_I$ is exactly the same as the typical 3D BHZ model [35–37], where H_I is attributed to the intrinsic SOC. For electrons, H_{RD} arises in conditions of broken inversion symmetry, which includes $\pm iC_2 k_\mp$ and $\mp iC_1 k_\pm$ terms, corresponding to the Rashba $(k_y\sigma_x - k_x\sigma_y)$ and Dresselhaus $(k_y\sigma_x + k_x\sigma_y)$ SOC, respectively. In analogy, H_I and H_{RD} are called the intrinsic and Rashba-Dresselhaus pseudo-SOC for phonon pseudospins. In this sense, phonons and electrons share essentially the same Hamiltonian, though their underlying physics is distinctly different. This implies a "duality" between phonon pseudospins and electron spins. Therefore, we can study the topological and quantum physics of phonon pseudospins by borrowing ideas from spintronics. This key result could lay the foundation for an emerging field of "pseudospin phononics".

Then we will discuss phononic topological properties by the effective Hamiltonian. When excluding H_{RD} and selecting $k_z = 0$, H reduces to the 2D BHZ model, which gives quantized pseudospin-resolved Chern numbers $\mathscr{C}_{\uparrow(\downarrow)}$ [38]. As type-I HSM exist in pairs, $\mathscr{C}_{\uparrow(\downarrow)} = \pm 2$ when a band inversion occurs (i.e., $M/B_1 > 0$). The sum of $\mathscr{C}^s = (\mathscr{C}_\uparrow - \mathscr{C}_\downarrow)/4$ contributed by all HSM mod 2 gives a topological invariant $\mathbb{Z}_2$. The 3D phononic TI phase is characterized by $\mathbb{Z}_2 = 1$. The inclusion of H_{RD} introduces intraband coupling between opposite pseudospins, which removes the pseudospin degeneracy except at the HSM. Then $\mathscr{C}_{\uparrow(\downarrow)}$ gets ill defined, but the $\mathbb{Z}_2$ topological classification remains valid [30]. The $\mathbb{Z}_2$ topological invariant will not be affected by H_{RD} as far as the bulk band gap keeps open when adiabatically turning on H_{RD}.

To demonstrate the nontrivial topological states, we explicitly studied lattice vibrations in a C_{6v} lattice [Figure 1(a)]. The interatomic interactions between the nearest and next-nearest neighbors were described by longitudinal and transverse force constants, as done previously [34]. The out-of-plane vibrations typically have minor influence on topological properties of in-plane vibrations [33], which are thus neglected for simplicity. We systematically searched the whole space of interatomic coupling parameters and found that the required band inversions can be obtained by a wide range of coupling parameters. Details of calculation methods and parameters related to the following discussions were described in Supplemental Material [33].

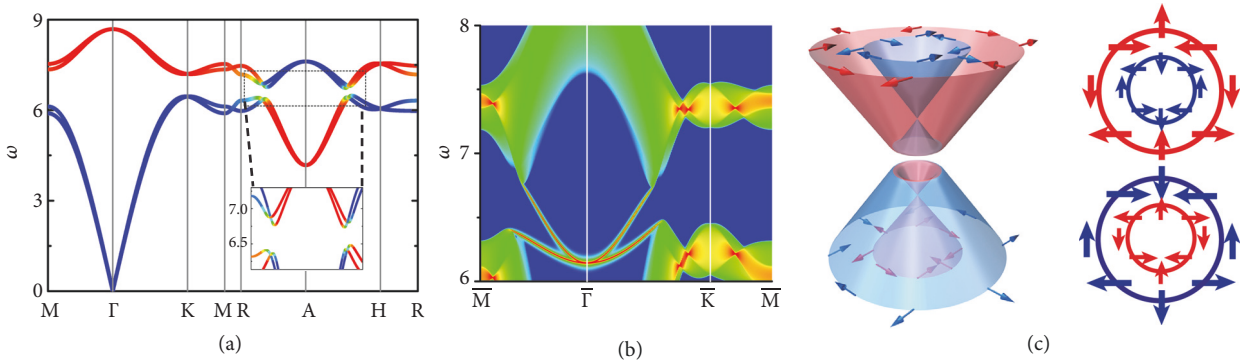


FIGURE 2: (a) Dispersion curves of a type-II phononic TI. Blue (red) color is used to denote the contribution of I (O) vibrational modes. (b) LDOS of the (001) surface, where higher (lower) LDOS are colored red (blue). (c) Schematic phonon dispersion and pseudospin textures in the $k_z = 0$ plane near A. The right panel displays pseudospin textures of O (top) and I (bottom) vibrational modes from the top view.

Figure 1(c) presents phonon dispersion curves with a band inversion between I and O vibrational modes at K. This band inversion leads to a nontrivial band topology $\mathbb{Z}_2 = 1$, as confirmed by our calculations of hybrid Wannier centers [39, 40] that display partner switching between Kramers-like pairs [33]. Moreover, there is a frequency gap between the two kinds of bands. The system is thus a 3D phononic TI. A hallmark of phononic TIs is the existence of gapless surface state within the bulk gap, which is topologically protected when the corresponding symmetry is preserved. On the (001) surface where the C_{6v} symmetry preserves, we indeed observed a single pair of gapless Dirac-cone-shaped surface bands located near $\overline{K}$ and $\overline{K'}$ [Figure 1(d)], as warranted by the bulk-boundary correspondence [41].

Figure 1(e) displays schematic pseudospin textures of bulk bands in the $k_z = 0$ plane. There would be no net pseudospin polarization if excluding the Rashba-Dresselhause pseudo-SOC interaction H_{RD}. Interestingly, when including H_{RD}, Rashba-like and Dresshause-like pseudospin textures evolve in the O and I bands, respectively. We further considered the topological surface states (TSSs) near the Dirac point, which are described by the effective Hamiltonian (referenced to the Dirac frequency) $H_{\text{surf}} = v_D(k_x\sigma_x\tau_z + k_y\sigma_y)$, where $\tau_z = \pm 1$ refers to K (K') valley; v_D is the group velocity at the Dirac point. Noticeably, H_{surf} of each valley has the same form as for TSSs of electrons [35], whose pseudospin textures are schematically displayed in Figure 3(a). By adiabatically varying $\mathbf{k}$ along the loop enclosing K (K'), the pseudospin vectors wind ± 1 times, giving quantized Berry phases of $\pm\pi$. The similarity between phonon pseudospins and electron spins is thus well demonstrated for both bulk and surface bands.

3. Type-II Phononic TIs

Type-II phononic TIs are characterized by the existence of band inversions at type-II HSM (Γ or A). Importantly, due to the C_6 rotation symmetry, all the linear terms of $k_\pm$ are forbidden in the effective Hamiltonian near type-II HSM, which is expressed as follows [33]:

$$H' = H_0 + H'_I + H'_{RD} = \begin{pmatrix} M_{\mathbf{k}} & \delta_1 k_-^2 & -ic_1 k_-^2 & \delta_2 k_z \\ \delta_1 k_+^2 & -M_{\mathbf{k}} & \delta_2 k_z & ic_2 k_+^2 \\ ic_1 k_+^2 & \delta_2 k_z & M_{\mathbf{k}} & -\delta_1 k_+^2 \\ \delta_2 k_z & -ic_2 k_-^2 & -\delta_1 k_-^2 & -M_{\mathbf{k}} \end{pmatrix}. \quad (3)$$

A new kind of intrinsic and Rashba-Dresselhaus pseudo-SOC (H'_I and H'_{RD}) is thus introduced.

Figure 2(a) presents dispersion curves of a type-II phononic TI, which is characterized by a band inversion at A, a finite frequency gap, and a nontrivial band topology $\mathbb{Z}_2 = 1$ verified by the calculations of hybrid Wannier centers [33]. We also calculated the surface states of the (001) termination [Figure 2(b)], which shows a quadratic band crossing at $\overline{\Gamma}$, in contrast to a pair of linear band crossings at type-I HSM. The type-II TSSs are described by the effective Hamiltonian (referenced to the degenerate frequency) $H'_{\text{surf}} = D[(k_x^2 - k_y^2)\sigma_x - 2k_xk_y\sigma_y]$, where D is a coefficient. Pseudospin textures of bulk bands [Figure 2(c)] are neither typical Rashba-like nor typical Dresselhaus-like, but display new pseudospin-momentum locked features. Pseudospin textures of type-II TSSs are significantly different from those of type-I TSSs [Figure 3(a)], which are characterized by winding numbers of ± 2 and quantized Berry phases of $\pm 2\pi$.

4. Pseudospin-Momentum Locked Phonon Transport

One prominent feature caused by the pseudo-SOC H_{RD} or H'_{RD} is that the pseudospin and momentum of phonons are locked, which plays an important role in determining transport properties. Moreover, type-I and type-II bulk/surface bands are featured by different kinds of pseudospin-momentum locking, leading to distinct transport behaviors. To demonstrate the concept, we simulated phonon transport of TSSs in tunneling junctions [33], where a tunneling barrier is introduced into the gate region as schematically displayed in Figure 3(a). The height of tunneling barrier, in principle, could be controlled by using a piezoelectric

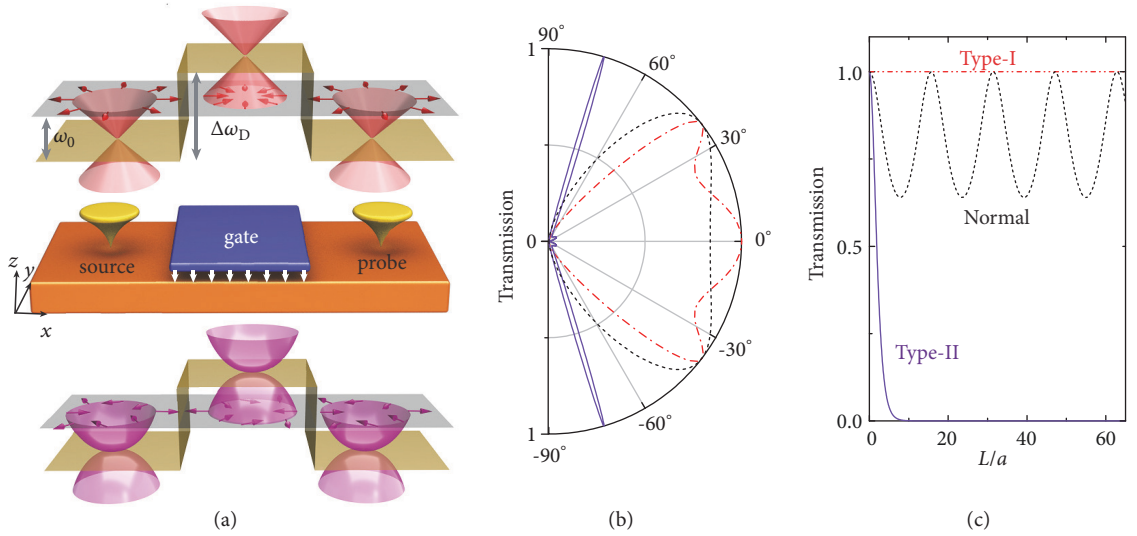


FIGURE 3: (a) Schematic phonon tunneling junction, where surface lattice vibrations of frequency ω_0 are excited (detected) by a point-like source (probe) and a tunneling barrier $\Delta\omega_D$ is applied by a piezoelectric gate. Schematic phonon dispersion and pseudospin textures of type-I (type-II) TSSs are displayed in the top (bottom) panel. (b) Phonon transmission as a function of incident angle θ for type-I TSSs (red dash-dotted), type-II TSSs (purple solid), and normal surface states (black dashed), for which we used barrier widths of = $132a$, $29.5a$, and $132a$, respectively. a is the length parameter depicted in Figure 1(a). $\theta = 0$ is defined along the x-axis. (c) Phonon transmission as a function of L for $\theta = 0$. $\omega_0 = 0.1$ and $\Delta\omega_D = 0.3$ were used.

gate that changes the on-site potential, strain, or interatomic coupling of surface atoms [26]. Figure 3(b) shows phonon transmissions as a function of incident angle θ for type-I and type-II TSSs. Normal surface states with a linear band dispersion and no pseudospin-momentum locking were also studied for comparison. Noticeably, there exists resonant phonon transport (transmission equal to 1) along some particular directions, which satisfy the constructive interference condition of Fabry-Pérot resonances, $q_x L = n\pi$, where q_x is the x-component of wavevector in the gate region (Supplemental Figure S3), L is the barrier width, and n is an integer number. Moreover, phonon transmission of normal surface states oscillates with varying L, which is also expected by the Fabry-Pérot physics.

However, substantially different results are found for type-I and type-II TSSs. Take $\theta = 0$ for example. $\theta = 0$ corresponds to transport along x-axis. Transport of type-I TSSs keeps ballistic, while phonon transmission of type-II TSSs decays exponentially with increasing L [Figure 3(c)]. These unconventional transport behaviors are insensitive to material details, indicating a topological origin. Importantly, these physical effects can be well understood by pseudospin physics. Specifically, for type-I (type-II) TSSs, the forward-moving phonon modes have the same (opposite) pseudospins between the upper and lower Dirac cones, which correspond to transport channels of the source/probe and gate, respectively [Figure 3(a)]. Because of the perfectly matched (mismatched) pseudospins, phonons are able to transport across the barrier with no (full) backscattering. These quantum transport phenomena are inherently related to the quantized Berry phase π (2π) of type-I (type-II) TSSs, which induces destructive (constructive) interferences between incident and backscattered waves.

Our findings suggest some potential applications of TSSs. For instance, the excellent transport ability of type-I TSSs can be utilized for low-dissipation phononic devices. The strongly angle-dependent transmission of type-II TSSs, which are confined to transport along some specific directions, can be used to design directional phononic antenna. Moreover, type-II TSSs are promising for building efficient phononic transistors, because their phonon conduction in the tunneling junction can be switched off (on) by a finite (zero) barrier.

5. Phononic Topological Semimetals

In addition to phononic TIs, topological band inversions can introduce other novel topological phases, including topological nodal-ring semimetals and topological Weyl semimetals, which are collectively called phononic topological semimetals. The essential physics is illustrated in Figure 4(a). Let us start from $H = H_0$ and take two pairs of bands inverted at K for example. Generally, the pseudospin degeneracy is split by H_{RD}, and a full band gap is induced by H_I, leading to phononic TIs. However, phononic topological semimetals would emerge if the opening of band gap was forbidden by symmetry. This is possible here, providing that band splittings of H_{RD} have opposite signs between I and O vibrational modes (i.e., $C_1C_2 > 0$). Then, when in the presence of mirror symmetry M_z (with the same atoms at A and B sites), the crossing rings in the $k_z = 0$ plane are protected to be gapless, introducing topological nodal-ring semimetals. In contrast, under broken M_z, the nodal rings are gapped out except for some gapless points that are protected to exist in the Γ-K line by mirror symmetry M_x. These gapless points are Weyl points, and the resulting phase is topological Weyl semimetal.

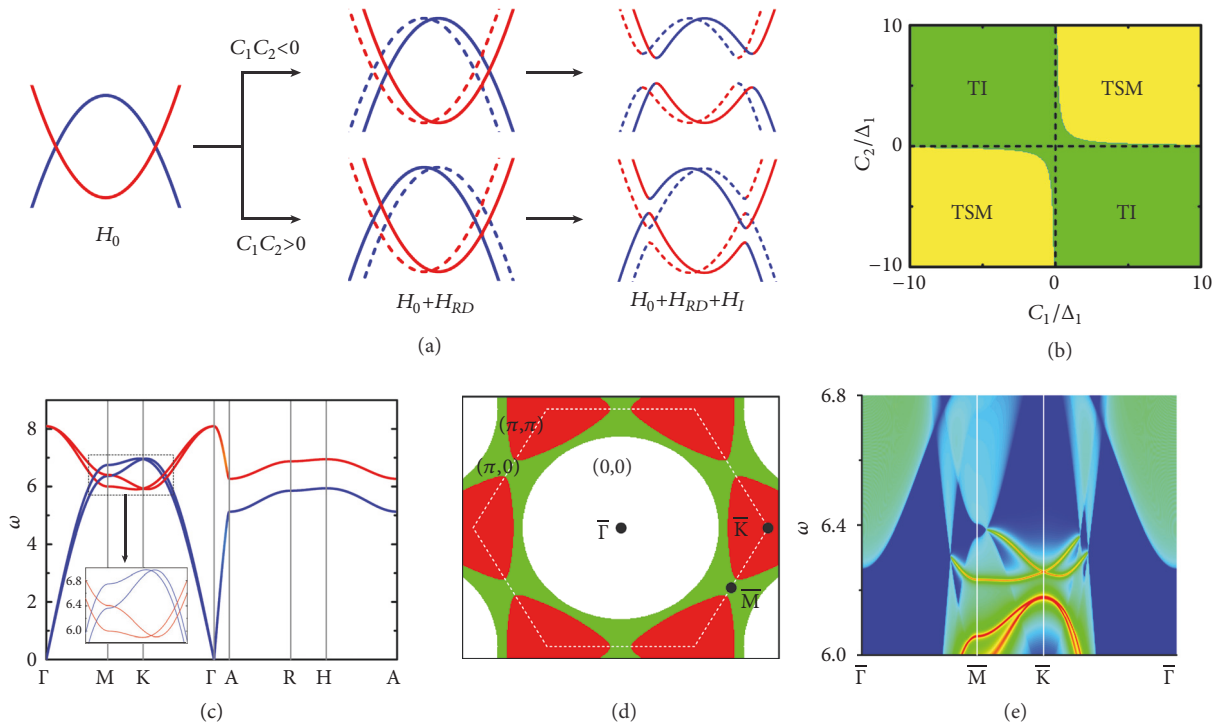


FIGURE 4: (a) Schematic evolution of I (blue) and O (red) vibrational bands near K under the influence of intrinsic pseudo-SOC H_I and Rashba-Dresselhause pseudo-SOC H_{RD}. The H_{RD}-induced pseudospin splittings of I and O vibrational bands have same (opposite) signs when $C_1C_2 < 0$ ($C_1C_2 > 0$), which can result in phononic TIs or topological semimetals (TSMs) as summarized in the topological phase diagram (b). (c) Dispersion curves of a phononic topological nodal-ring semimetal. Blue (red) color is used to denote the contribution of I (O) vibrational modes. (d) Zak phases along the (001) direction of the lowest two bands for the 2D surface BZ. (e) LDOS of the (001) surface, where higher (lower) LDOS are colored red (blue).

A unified description of these topological phases is provided by the phase diagram presented in Figure 4(b).

Figure 4(c) presents dispersion curves of a phononic topological nodal-ring semimetal protected by M_z, for which equivalent A and B sites were selected [33]. The gapless feature in the $k_z = 0$ plane is consistent with the symmetry analysis. Moreover, we calculated the Zak phase θ_{Zak} along the (001) direction for the 2D surface BZ, where θ_{Zak} has quantized values of 0 or π [Figure 4(d)]. The nodal rings appear at boundaries between regions of $\theta_{\text{Zak}} = 0$ and $\theta_{\text{Zak}} = \pi$, implying their topological nature. Furthermore, phononic drumhead surface states were observed by our surface-state calculations [Figure 4(e)], which is a hallmark feature of topological nodal-ring semimetals. Their evolution with varying phonon frequencies are displayed in Supplemental Figure S5.

6. Guiding Principles for Searching Candidate Materials

We would like to provide guiding principles for searching candidate materials by first-principles calculations: (i) For a family of materials having a specified crystalline symmetry, use group theory to determine band degeneracies at high symmetry momenta (HSM). Topological phononic states would be allowed, if having band degeneracies at more than one HSM. (ii) For a specific material, calculate the phonon dispersion and eigenstates at HSM. Sort degenerate bands at each HSM according to their phonon frequencies. Then check whether the order of degenerate bands with different irreducible representations varies between different HSM. If so, a topological band inversion usually exists. (iii) For the material with a topological band inversion, calculate the phonon dispersion in the whole momentum space. Thus, whether it is a topological insulator or semimetal can be defined. (iv) Determine the topological nature explicitly by computing hybrid Wannier centers and topological surface states. The simple guiding principles could be applied for high throughput discovery of phononic topological materials.

7. Experimental Signatures of Topological Phononic Materials

Hallmarks of a topological phononic material include (i) the existence of topological band inversion for bulk phonon modes at HSM and (ii) the existence of topologically protected, gapless phononic states on the boundary. One can use infrared spectroscopy, Raman techniques, or inelastic neutron scattering to detect bulk phonon modes at HSM. The measured band degeneracy and band order at HSM could be used to determine topological band inversion. Besides, one can use angle-resolved electron energy loss

spectroscopy that is a surface-sensitive technique to measure phonon dispersion of surfaces. Thus topological boundary states of phonons can be directly probed. These experimental signatures in combination with first-principles calculations could be used to determine topological nature of specific materials.

8. Outlook

Our work sheds lights on future study of topological phononics. A few promising research directions are opened: (i) To search for new symmetry-protected phononic topological states. In addition to C_{nv}, there are many other symmetries, like (magnetic) space group symmetry, time reversal symmetry, particle-hole symmetry, etc., and their combinations, which could result in rich topological phases [28, 42]. (ii) To explore novel physical effects by breaking symmetry locally or globally. For instance, the quantum anomalous Hall-like states would emerge if time reversal symmetry breaking effects were introduced to 2D TSSs of phononic TIs. (iii) To investigate unconventional electron-phonon coupling and superconductivity caused by the pseudospin- and topology-related physics of phonons. Many material systems could simultaneously host nontrivial topological states of electrons and phonons. Thus, TSSs of electrons and phonons are able to coexist on the material surfaces. Their interactions might be exotic, for instance, due to the (pseudo-)spin-momentum locking. (iv) To find realistic candidate materials for experiment and application. Very few realistic materials of chiral phonons [21, 34, 43] and phononic topological semimetals [22–25] have been reported, and plenty of unknown candidate materials of various phononic topological phases are awaiting to be discovered. It is helpful to develop machine learning methods for high throughput discovery of phononic topological materials.

Conflicts of Interest

The authors declare that there are no conflicts of interest regarding the publication of this article.

Acknowledgments

This work was supported by the Basic Science Center Project of NSFC (Grant No. 51788104), the and Ministry of Science Technology of China (Grants No. 2016YFA0301001, No. 2018YFA0307100, and No. 2018YFA0305603), the National Natural Science Foundation of China (Grants No. 11874035, No. 11674188, and No. 11334006), and the Beijing Advanced Innovation Center for Future Chip (ICFC).

Supplementary Materials

(I) Derivation of effective Hamiltonians, (II) topological phase diagram, (III) interatomic coupling parameters, (IV) hybrid Wannier centers, (V) pseudospin textures, (VI) phonon transport in tunneling junctions, (VII) influence of out-of-plane vibrations, and (VIII) phononic topological semimetal. *(Supplementary Materials)*

References

[1] E. Prodan and C. Prodan, "Topological phonon modes and their role in dynamic instability of microtubules," *Physical Review Letters*, vol. 103, no. 24, Article ID 248101, 2009.

[2] L. Zhang, J. Ren, J.-S. Wang, and B. Li, "Topological nature of the phonon hall effect," *Physical Review Letters*, vol. 105, no. 22, Article ID 225901, 2010.

[3] Y.-T. Wang, P.-G. Luan, and S. Zhang, "Coriolis force induced topological order for classical mechanical vibrations," *New Journal of Physics*, vol. 17, Article ID 073031, 2015.

[4] P. Wang, L. Lu, and K. Bertoldi, "opological phononic crystals with one-way elastic edge waves," *Physical Review Letters*, vol. 115, no. 10, Article ID 104302, 2015.

[5] Z. Yang, F. Gao, X. Shi et al., "Topological acoustics," *Physical Review Letters*, vol. 114, no. 11, Article ID 114301, 2015.

[6] A. B. Khanikaev, R. Fleury, S. H. Mousavi, and A. Alù, "Topologically robust sound propagation in an angular-momentum-biased graphene-like resonator lattice," *Nature Communications*, vol. 6, Article ID 8260, 2015.

[7] X. Ni, C. He, X.-C. Sun et al., "Topologically protected one-way edge mode in networks of acoustic resonators with circulating air flow," *New Journal of Physics*, vol. 17, Article ID 053016, 2015.

[8] V. Peano, C. Brendel, M. Schmidt, and F. Marquardt, "Topological phases of sound and light," *Physical Review X*, vol. 5, no. 3, Article ID 031011, 2015.

[9] T. Kariyado, Y. Hatsugai, and Sci. Rep, "Manipulation of dirac cones in mechanical graphene," *Scientific Reports*, vol. 5, Article ID 18107, 2015.

[10] R. Fleury, A. B. Khanikaev, and A. Alù, "Floquet topological insulators for sound," *Nature Communications*, vol. 7, Article ID 11744, 2016.

[11] R. Süsstrunk and S. D. Huber, "Classification of topological phonons in linear mechanical metamaterials," *Proceedings of the National Academy of Sciences of the United States of America*, vol. 113, no. 33, pp. E4767–E4775, 2016.

[12] S. D. Huber, "Topological mechanics," *Nature Physics*, vol. 12, pp. 621–623, 2016.

[13] Y. Liu, Y. Xu, S.-C. Zhang, and W. Duan, "Model for topological phononics and phonon diode," *Physical Review B: Condensed Matter and Materials Physics*, vol. 96, no. 6, Article ID 064106, 2017.

[14] Y. Liu, Y. Xu, and W. Duan, "Berry phase and topological effects of phonons," *National Science Review*, vol. 5, p. 314, 2017.

[15] H. Abbaszadeh, A. Souslov, J. Paulose, H. Schomerus, and V. Vitelli, "Sonic landau levels and synthetic gauge fields in mechanical metamaterials," *Physical Review Letters*, vol. 119, no. 19, Article ID 195502, 1955.

[16] R. Süsstrunk and S. D. Huber, "Observation of phononic helical edge states in a mechanical topological insulator," *Science*, vol. 349, no. 6243, pp. 47–50, 2015.

[17] S. H. Mousavi, A. B. Khanikaev, and Z. Wang, "Topologically protected elastic waves in phononic metamaterials," *Nature Communications*, vol. 6, Article ID 8682, 2015.

[18] L.-H. Wu and X. Hu, "Scheme for achieving a topological photonic crystal by using dielectric material," *Physical Review Letters*, vol. 114, no. 22, Article ID 223901, 2015.

[19] R. K. Pal, M. Schaeffer, and M. Ruzzene, "Helical edge states and topological phase transitions in phononic systems using bi-layered lattices," *Journal of Applied Physics*, vol. 119, no. 8, Article ID 084305, 2016.

[20] C. He, X. Ni, H. Ge et al., "Acoustic topological insulator and robust one-way sound transport," *Nature Physics*, vol. 12, pp. 1124–1129, 2016.

[21] Y. Liu, C.-S. Lian, Y. Li, Y. Xu, and W. Duan, "Pseudospins and topological effects of phonons in a kekulé lattice," *Physical Review Letters*, vol. 119, no. 25, Article ID 255901, 2017.

[22] T. Zhang, Z. Song, A. Alexandradinata et al., "Double-weyl phonons in transition-metal monosilicides," *Physical Review Letters*, vol. 120, Article ID 016401, 2018.

[23] H. Miao, T. T. Zhang, L. Wang et al., "Observation of double weyl phonons in parity-breaking FeSi," *Physical Review Letters*, vol. 121, no. 3, Article ID 035302, 2018.

[24] J. Li, Q. Xie, S. Ullah et al., "Coexistent three-component and two-component Weyl phonons in TiS, ZrSe, and HfTe," *Physical Review B: Condensed Matter and Materials Physics*, vol. 97, no. 5, Article ID 054305, 2018.

[25] Q. Xie, J. Li, M. Liu et al., "Phononic weyl nodal straight lines in high-temperature superconductor MgB_2," 2018, https://arxiv.org/abs/1801.04048.

[26] N. Li, J. Ren, L. Wang, G. Zhang, P. Hänggi, and B. Li, "*Colloquium*: Phononics: Manipulating heat flow with electronic analogs and beyond," *Reviews of Modern Physics*, vol. 84, no. 3, p. 1045, 2012.

[27] L. Fu, C. L. Kane, and E. J. Mele, "Topological insulators in three dimensions," *Physical Review Letters*, vol. 98, no. 10, Article ID 106803, 2007.

[28] C.-X. Liu, R.-X. Zhang, and B. K. VanLeeuwen, "Topological nonsymmorphic crystalline insulators," *Physical Review B*, vol. 90, no. 8, Article ID 085304, 2014.

[29] X.-Y. Dong and C.-X. Liu, "Classification of topological crystalline insulators based on representation theory," *Physical Review B*, vol. 93, no. 4, Article ID 045429, 2016.

[30] L. Fu, "Topological crystalline insulators," *Physical Review Letters*, vol. 106, no. 10, Article ID 106802, 2011.

[31] A. Alexandradinata, C. Fang, M. J. Gilbert, and B. A. Bernevig, "Spin-orbit-free topological insulators without time-reversal symmetry," *Physical Review Letters*, vol. 113, no. 11, Article ID 116403, 2014.

[32] M. S. Dresselhaus, G. Dresselhaus, and A. Jorio, *Group Theory: Application to the Physics of Condensed Matter*, Springer, Berlin, Germany, 2008.

[33] See Supplemental Material for details of calculation methods and parameters.

[34] L. Zhang and Q. Niu, "Chiral phonons at high-symmetry points in monolayer hexagonal lattices," *Physical Review Letters*, vol. 115, no. 11, Article ID 115502, 2015.

[35] H. Zhang, C. X. Liu, X. L. Qi, X. Dai, Z. Fang, and S. C. Zhang, "Topological insulators in Bi_2Se_3, Bi_2Te_3 and Sb_2Te_3 with a single Dirac cone on the surface," *Nature Physics*, vol. 5, no. 6, pp. 438–442, 2009.

[36] X.-L. Qi and S.-C. Zhang, "The quantum spin Hall effect and topological insulators," *Physics Today*, vol. 63, no. 1, p. 33, 2010.

[37] X.-L. Qi and S.-C. Zhang, "Topological insulators and superconductors," *Reviews of Modern Physics*, vol. 83, no. 4, Article ID 1057, 2011.

[38] C. L. Kane and E. J. Mele, "Quantum spin hall effect in graphene," *Physical Review Letters*, vol. 95, no. 22, Article ID 226801, 2005.

[39] M. Taherinejad, K. F. Garrity, and D. Vanderbilt, "Wannier center sheets in topological insulators," *Physical Review B*, vol. 89, no. 11, Article ID 115102, 2014.

[40] A. Alexandradinata, X. Dai, and B. A. Bernevig, "Wilson-loop characterization of inversion-symmetric topological insulators," *Physical Review B*, vol. 89, no. 15, Article ID 155114, 2014.

[41] M. Z. Hasan and C. L. Kane, "*Colloquium*: topological insulators," *Reviews of Modern Physics*, vol. 82, no. 4, Article ID 3045, 2010.

[42] C. Fang and L. Fu, "New classes of three-dimensional topological crystalline insulators: Nonsymmorphic and magnetic," *Physical Review B*, vol. 91, no. 16, Article ID 161105, 2015.

[43] H. Zhu, J. Yi, M. Y. Li et al., "Observation of chiral phonons," *Science*, vol. 359, no. 6375, pp. 579–582, 2018.